Contract No.:

This manuscript has been authored by Savannah River Nuclear Solutions (SRNS), LLC under Contract No. DE-AC09-08SR22470 with the U.S. Department of Energy (DOE) Office of Environmental Management (EM).

Disclaimer:

The United States Government retains and the publisher, by accepting this article for publication, acknowledges that the United States Government retains a non-exclusive, paid-up, irrevocable, worldwide license to publish or reproduce the published form of this work, or allow others to do so, for United States Government purposes.

Analysis of Powder Airborne Release Fractions for Vessel Ruptures

James E. Laurinat[1]
Savannah River National Laboratory
Savannah River Site
Aiken, South Carolina 29808
james.laurinat@srnl.doe.gov

Steve J. Hensel
Savannah River Nuclear Solutions LLC
Savannah River Site
Aiken, South Carolina 29808
steve.hensel@srnl.doe.gov
ASME Fellow

ABSTRACT

The Department of Energy (DOE) handbook for airborne releases from nonreactor nuclear facilities bases its bounding airborne release fraction (ARF) for pressurized powders on tests conducted at Pacific Northwest Laboratory (PNL). An analysis is presented that correlates the ARF from these tests. The amount of powder that becomes airborne is correlated in terms of an adjusted airborne release fraction (AARF) equal to the product of the powder entrainment from the powder bed and the ratio of the total vessel volume to the volume occupied by the powder bed. Powder entrainments and release fractions at low pressures are correlated using a fluidized bed analogy. The analysis shows that the entrainment is enhanced by a sonic shock if the pressure prior to the rupture exceeds approximately 33 psig. A secondary, three-dimensional shock is predicted to occur at an initial pressure of approximately 332 psig. A correlation based on this analysis is used to predict the ARF for ruptures of vessels containing plutonium oxide. It is assumed that the oxide is pressurized by hydrogen that is radiolytically generated from adsorbed moisture.

INTRODUCTION

The DOE Handbook for airborne releases from nonreactor facilities [1] recommends the use of an ARF of 0.10 (10%) for sudden depressurizations of vessels containing powders. The recommended ARF bounds release rates measured by Sutter et al. at PNL for titanium dioxide (TiO_2) and depleted uranium oxide (U_3O_8) powders. [2,3,4] PNL conducted two sets of powder release tests, In the first set of tests, the so-called Pressurized Airborne Release Equipment (PARE) tests, the oxide powder was placed in a vessel with a top that was sealed by a series of two rupture disks, as shown by Fig. 1. During the PARE tests, the vessel was pressurized by air flow to a pressure exceeding the rupture disk pressure. The space between the rupture disks then

was evacuated, causing both disks to rupture. Upon rupture; the fractional powder release was then measured. The second set of tests, the so-called Powder Releases Above Chamber (PRAC) tests, differed from the PARE tests in that the air space below the powder chamber was pressurized. The two rupture disks were situated between the pressurized air space and the powder vessel, which had an open top. The DOE Handbook cited the PARE tests as being representative of typical pressurized powder releases and therefore used bounding release rates from these tests to establish the ARF.

The powder entrainment analysis presented in this report assumes that the gas and solid particles in the oxide layer mixed only with the gas in the space above the oxide layer inside the basket. The analysis demonstrates that, with a reasonable set of assumptions, this mixing accounts for the measured powder entrainment, i.e., the measured ARF.

DESCRIPTION OF PARE TESTS

The analysis of airborne releases is based on the PARE tests. The PARE, depicted in Fig. 1, had a total volume of approximately 0.0008 m^3 and could be loaded with 0.000524 m^3 of powder. A charge of 0.350 kg of TiO$_2$ powder filled the chamber. A double rupture disk system was used. This system allowed the intermediate chamber to be pressurized so that the pressure differential across each rupture disk was less than the rupture pressure, while the total pressure differential across both disks exceeded the rupture pressure. During a test, a solenoid valve was activated, to evacuate the intermediate chamber. This caused the lower disk to rupture first, followed by rupture of the upper disk.

To collect powder samples, samplers were immediately turned on to pull air through high volume filters and impactors. The sampling room was approximately 3 m high and 2.9 m in diameter, for a total room volume of about 20 m^3. The sampling arrangement is shown by Fig. 2.

PARE tests were run with either 0.100 kg or 0.350 kg of powder in the test chamber, at pressures ranging from 9 psig to 500 psig. Tables 1 and 2 summarize the results of the PARE tests.

A cursory review of the PARE test conditions indicates that they are representative of a pressurized release due to a postulated rupture of a vessel or vial containing plutonium dioxide (PuO$_2$) powder. The porosity and particle size of the powders used by PNL are nearly the same as for a typical PuO$_2$ powder. The estimated porosity of the TiO$_2$ powder, based on a calculated bulk density of 667 kg/m^3, was 0.843, which translates to a PuO$_2$ bulk density of 1800 kg/m^3, typical of powders encountered at the Savannah River Site (SRS). The average particle size for the TiO$_2$ and U$_3$O$_8$ powders was approximately 10 microns, again typical of SRS PuO$_2$ powders.

The only aspect of the PARE tests that might not simulate a postulate rupture and release from an SRS vessel was the placement of the powder. The powder was placed in a basket with a perforated bottom that was covered by filter paper. Air was introduced into a chamber below the basket. It is presumed that there was minimal air flow into the test chamber during the depressurization transient due to the short duration of this transient and that, therefore, the entire vessel could be considered to be closed during the depressurization. However, it is not known to what extent the powder was lifted off the bottom of the basket during depressurization or what effect any lifting had on the entrainment of airborne powder particles.

POWDER ENTRAINMENT ANALYSIS

The analysis of powder entrainment is based on the assumption that the entrainment is controlled by the carrying capacity of the gas. It is assumed that, following a vessel rupture, the

gas almost immediately accelerates to its quasi-steady state exit velocity, which, for sufficiently high pressures, is the sonic velocity. The gas then accelerates the powder particles to a somewhat lower velocity. The ratio between the gas and solid particle velocities, called the slip ratio, is determined from an energy balance for the acceleration of the solids. The energy balance, which is weighted by the relative mass flow rates of the gas and solids, relates the cumulative energy of the solids flow to the work performed by the gas flow to accelerate the particles. This energy balance takes the form

$$W_s v_s^2 = W_g v_g \left(v_g - v_s \right) \tag{1}$$

In terms of the slip ratio, the energy balance is given by

$$\frac{W_s}{W_g} = s_f \left(s_f - 1 \right) \tag{2}$$

If the heat transfer during the depressurization transient is restricted to the gas phase, as it should be for rapid depressurization, then the energy balance for the depressurization becomes

$$m_g h_0 = m_g h + \frac{1}{2} W_g v_g + \frac{1}{2} W_s v_s \tag{3}$$

Eq. 3 simplifies to

$$h_0 = h + \frac{1}{2} v_g^2 \left(1 + \frac{W_s}{W_g s_f} \right) \tag{4}$$

To close the energy balance for the depressurization, the flow of entrained solids must be related to the gas flow. Depressurization initiates gas flow out of the vessel, which in turn accelerates the powder particles. If the initial pressure prior to the rupture is sufficiently high, then the rupture will produce a sonic shock in the vessel. It is appropriate to assume that the energy transfer for intense mixing due to a shock would be limited so that, after mixing, the energy initially present in the gas phase is distributed evenly between the gas and solid phases. This implies that the upper limit for the flow of entrained solids is given by

$$\frac{W_s}{W_g s_f} = 1 \tag{5}$$

Solution of Eqs. 2 and 5 gives, for the slip ratio and the solid entrainment ratio,

$$s_f = 2 \tag{6}$$

and

$$\frac{W_s}{W_g} = 2 \tag{7}$$

In the absence of a sonic shock, the entrainment of solids during depressurization resembles entrainment in a fluidized bed. At the critical flow for the onset of fluidization, Matsen gives a slip ratio of 1.293. [5] This slip ratio represents the ratio of the gas velocity to the settling velocity for a single particle. If it is assumed that this slip ratio represents the amount of energy that must be transferred from the gas to the powder to begin fluidization, then, at high velocities, where gravitational effects are negligible, the same value also applies to the actual ratio of gas to solid velocities. Thus, without a shock,

$$s_f = 1.293 \tag{8}$$

and

$$\frac{W_s}{W_g} = 0.379 \tag{9}$$

The critical pressure for the appearance of a two-phase shock can be estimated by solving the energy balance for entrained particle flow. From Eqs. 4 and 5,

$$h_0 = h + v_g{}^2 \tag{10}$$

Since heat transfer is restricted to the gas phase during the depressurization,

$$h_0 = c_p T_0 = \frac{k R_g T_0}{(k-1)} \tag{11}$$

and

$$h = c_p T = \frac{k R_g T}{(k-1)} \tag{12}$$

It is convenient to express the solution of Eqs. 10, 11, and 12 in terms of the Mach number, defined by

$$M = \frac{v_g}{c} \tag{13}$$

The sonic velocity is calculated at conditions downstream from the shock, from the isentropic relation [6]

$$c^2 = k R_g T \tag{14}$$

From Eqs. 10 through 14, the temperature ratio across the shock is given by

$$\frac{T_0}{T} = 1 + (k-1)M^2 \tag{15}$$

The corresponding pressure ratio for isentropic flow is [6]

$$\frac{P_0}{P} = \left(1 + (k-1)M^2\right)^{k/(k-1)} \tag{16}$$

For a Mach number M equal to one, this simplifies to

$$\frac{P_0}{P} = k^{k/(k-1)} \tag{17}$$

It may be noted that this pressure ratio exceeds the ratio for isentropic single-phase gas flow, which is [6]

$$\frac{P_0}{P} = \left(\frac{k+1}{2}\right)^{k/(k-1)} \tag{18}$$

The critical pressure required for a two-phase shock in air is 0.329 MPa (33.0 psig). The corresponding pressure for a single-phase shock is 0.192 MPa (13.1 psig).

At high pressures, it is postulated that a secondary shock occurs that redirects the gas flow from a unidirectional flow at sonic velocity to a three-dimensional sonic flow. It is assumed that the three dimensional flow exhibits spherical symmetry, such that the cross-sectional flow surface goes from a flat circle to a sphere of the same diameter. Because the surface area of a sphere is four times the area of a circle of the same diameter, the kinetic energy term in the energy balance represented by Eqs. 3 and 4 quadruples. Therefore, the enthalpy after the secondary shock is related to the stagnation enthalpy by

$$h_0 = h + 2v_g^2 \left(1 + \frac{W_s}{W_g s_f} \right) \tag{19}$$

The secondary shock also would redirect the flow of entrained particles, from a single direction to a uniform distribution in six outward directions. One of these directions would return the particles to the powder bed surface, however, in effect cancelling out 1/6 of the energy due to entrainment from the original shock. The remaining 5/6 of the flow would maintain the energy level due to entrainment from the one-dimensional shock. Thus, ratio of the energy of the entrained particles to the energy for the gas flow becomes

$$\frac{W_s}{W_g s_f} = \frac{5}{6} \tag{20}$$

Solution of Eqs. 2 and 20 gives, for the secondary shock,

$$s_f = \frac{11}{6} \tag{21}$$

and

$$\frac{W_s}{W_g} = \frac{55}{36} = 1.528 \tag{22}$$

The pressure at which the secondary shock first appears can be calculated from an analysis similar to that in Eqs. 10 through 17. This analysis, applied to Eqs. 19 and 20, yields, for the secondary shock,

$$\frac{P_0}{P} = \left(\frac{11k - 8}{3} \right)^{k/(k-1)} \tag{23}$$

The critical pressure required for the secondary shock in air is computed to be 2.388 MPa (331.7 psig).

The entrainment ratio is expressed in terms of the gas and pycnometric solid densities, the gas and powder volumes, and the powder bed void fraction by

$$\frac{W_s}{W_g} = \frac{\rho_s V_s (1 - \varepsilon)}{\rho_{g,0} \left(V_s \varepsilon + m_f (V_t - V_s) \right)} \tag{24}$$

A mixing effectiveness factor is included in Eq. 24 to account for imperfect mixing when the volume of the gas exceeds the volume of the powder bed. This effectiveness factor is evaluated empirically from the Sutter et al. data [2,3] by requiring the entrainment fractions for varying powder fill fractions to converge to a single value at high pressures, where it may be assumed that the depressurization shock results in thorough mixing of the gas and the powder. Effectiveness factors were determined by trial and error. For the test with 0.350 kg TiO_2 powder, Sutter et al. state that the inner can was completely filled with powder, so there was no empty gas space. The individual mixing factors for the tests with 0.350 kg U_3O_8 powder, 0.100 kg TiO_2 powder, and 0.100 kg U_3O_8 powder were determined to be 1.0, 0.70, and 0.55, respectively.

Using these individual mixing factors, the mixing effectiveness factor is correlated as a function of the logarithm of the ratio of the total volume to the powder bed volume. The following expression gives a linear correlation, with the desirable feature of going to zero as the powder bed volume approaches zero, as shown by Fig. 3.

$$m_f = min\left(1, 0.7959\left(ln\left(\frac{V_t}{V_s}\right)\right)^{-0.55}\right) \tag{25}$$

It may be noted that the effectiveness factor for the 0.350 kg U_3O_8 test is equal to the maximum value of one. The gas space volume was almost equal to the powder bed volume for this test. If the same reasoning used to approximate the limiting entrainment is applied, a shock should be just sufficient to mix equal volumes of powder and gas, so that the effectiveness factor would be almost exactly equal to one, and the use of the data point in the correlation should be valid.

The form of the empirical correlation given by equation 27 is based on a mixing analogy. It may be assumed that the ratio of the bulk powder volume to the total vessel volume scales as the rate of mixing between these two volumes and that the effectiveness factor functions as a mixing depth for the degree of mixing of the powder volume with the total vessel volume. The mixing of the powder with the free gas in the vessel is a dispersion process, with a rate of mixing that is proportional to the function $exp\left(-x^2\right)$, where x is the distance from the powder/bulk gas interface, or the mixing depth. Inversion of this function gives an effectiveness factor that is proportional to the square root of the logarithm of the mixing rate, or powder volume fraction, in approximate agreement with Eq. 27.

The adjusted entrainment ratios calculated with the mixing effectiveness factor converge to a single value at initial pressures of 1.825 MPa (250 psig) and 3.549 MPa (500 psig), as shown by Fig. 4.

In addition to comparing the adjusted gas loadings for the Sutter et al. tests, Fig. 4 also plots the predicted gas loadings at high pressures (from Eq. 7) and at low pressures (from Eq. 9). The predicted loading for high pressures covers pressures between the predicted two-phase choked flow transition of 0.329 MPa (33.0 psig) (from Eq. 17) and the postulated transition to a secondary, three-dimensional shock at 2.388 MPa (331.7 psig) (from Eq. 23), and the predicted loading for low pressures is assumed to apply in the range between the predicted two-phase choked flow transition and the gas phase transition (from Eq. 18). The predicted loading following the postulated secondary shock (from Eq. 22) is bounded by the loading for a one-dimensional shock and therefore is not used to compute the ARF at high pressures. At 1.825 MPa (250 psig) and 3.549 MPa (500 psig), the predicted powder loadings approximately equal the average adjusted measured loadings. The measured values exhibit considerable scatter at 0.446 MPa (50 psig). At lower pressures, between the choked flow transitions for single-phase gas flow and two-phase flow, the predicted loading serves as an upper asymptote to the adjusted measured loadings. Very little entrainment was detected below the choked flow transition for gas flow.

Table 3 lists the powder entrainment ratios for the Sutter et al. data computed from Eq. 24, using the empirically determined mixing factors. This table also lists the average, the standard deviation, and the 95% one-sided confidence bound for the 0.446 MPa (50 psig), 1.825 MPa (250 psig), and 3.549 MPa (500 psig) tests. This confidence bound is used in formulating a bounding correlation for the entrainment ratio at high pressures, where it is predicted that entrainment is enhanced by the presence of a sonic shock. Uncertainties are not applied below the shock threshold pressure of 0.329 MPa (33.0 psig). Instead, based on the results shown in Fig. 4, the predicted entrainment ratio is applied as the bounding result in this lower pressure range.

The confidence bound is calculated using the Student's t distribution with three degrees of freedom. [7] The 95% confidence bound equals the average plus 2.353 times the standard deviation. The expression for the 95% confidence bound is

$$\left.\frac{W_s}{W_g}\right|_{95\%,P_i} = \left\langle \frac{W_s}{W_g} \right\rangle_{P_i} + 2.353\,\sigma \left(\frac{W_s}{W_g} \right)_{P_i} \tag{26}$$

The 95% confidence level upper bound is correlated as a function of its deviation from the predicted mass entrainment ratio of two, as shown by Fig. 5.

The power law correlation from Fig. 5 takes the form

$$\left.\frac{W_s}{W_g}\right|_{95\%} - 2 = 0.5059\,P_{ga}^{-0.964} \tag{27}$$

Eq. 26 is used to interpolate upper bound entrainment ratios between 0.446 MPa (50 psig) and 1.825 MPa (250 psig) and to extrapolate from 0.446 MPa (50 psig) to the predicted limiting pressure for the appearance of a shock, 0.329 MPa (33.0 psig), and to extrapolate above 3.549 MPa (250 psig).

APPLICATION OF PREDICTED ARF

The predicted ARF is computed by multiplying the predicted entrainment ratio given by Eq. 7 or Eq. 9 by the ratio of the mass of gas that mixes with the powder to the total mass of the powder. An upper limit of 1.0 is included to explicitly ensure that no more than all the powder is entrained. The resulting formula for the ARF is

$$ARF = min\left(1, \frac{W_s}{W_g}\left(\frac{\varepsilon V_s}{V_t} + m_f\left(1 - \frac{V_s}{V_t} \right) \right) \frac{\rho_{g,0} V_t}{\rho_s V_s (1-\varepsilon)} \right) \tag{28}$$

The ARF depends on the composition of the gas and powder in the vessel prior to rupture. One accident scenario that would result in an airborne release is exposure to a fire of a vessel containing plutonium dioxide powder with adsorbed moisture. In this scenario, evaporation of the adsorbed moisture and heat of the air initially inside the vessel would pressurize the vessel until it bursts. The gas density for this scenario is computed from the partial pressures and densities of air and water vapor, using the following ideal gas relation

$$\rho_{g,0} = \frac{M_{air}P_{air}}{R_g T_0} + \frac{M_{H_2O}P_{v,H_2O}}{R_g T_0} \tag{29}$$

The air partial pressure due to heating is given by

$$P_{air} = P_a\left(\frac{T_0}{T_a} \right) \tag{30}$$

The water vapor pressure is given by an Antoine formula: [8]

$$P_{v,H_2O} = \left(\frac{14.696}{760} \right)10^{\left(A - \frac{B}{T_0 - T_r + C} \right)} \tag{31}$$

where

$A = 8.07131, B = 1730.63, C = 233.426$ when $273.15 < T_0 < 373.15$,

$A = 8.14019, B = 1810.94, C = 244.485$ when $T_0 > 373.15$ (32)

The powder void fraction for the PuO$_2$ powder is assumed to be the same as that estimated for TiO$_2$ powder used in the Sutter et al. tests, which was 0.843. This void fraction yields a bulk density of 1800 kg/m^3 for PuO$_2$ powder.

DISCUSSION OF RESULTS

Using Eq. 28, contour plots have been calculated for the best estimate ARF as a function of temperature and pressure. As explained previously, this equation assumes that moisture-laden PuO$_2$ powder is stored in a vessel that bursts. It is assumed that the void fraction of the powder is the same as that of the TiO$_2$ powder used in the Sutter et al. tests; this void fraction yields a bulk density of 1800 kg/m^3. The pressure is calculated as a function of temperature under the assumption that heating results in evaporation of moisture to give a saturated vapor pressure in air. Figs. 6 and 7 plot the predicted ARF as functions of the oxide fill fraction and either temperature or pressure for the high pressure range above the transition to choked two-phase flow. The predicted ARF corresponds to the horizontal dotted line in Fig. 4.

Figs. 8 and 9 plot the predicted ARF for the pressure range between the transitions to choked gas flow and choked two-phase flow. The ARF in this case corresponds to the horizontal short dash-dotted line in Fig. 4.

At the same pressures, the ARF's calculated for PuO$_2$ powder are lower than the values measured by Sutter et al. because the density of PuO$_2$ is higher than the density of either TiO$_2$ or U$_3$O$_8$ and because the gas density is lower than for the Sutter et al. tests. The gas density is lower because the gas for the PuO$_2$ powder releases is assumed to be heated to the saturation vapor pressure of water (which approaches the total pressure) and because most of the gas for PuO$_2$ powder releases is water vapor (with a molecular mass of 0.018 kg/mole) rather than air (with an average molecular mass of 0.029 kg/mole).

As explained, the ARF values in Figs. 6 through 9 represent best estimate values for particle entrainment as a function of the oxide powder fill fraction and either the pressure or the temperature. To obtain a more useful correlation that can be applied in a dose/consequence analysis, it is desirable to simplify the ARF correlation to a bounding correlation that is a function of pressure only. This is accomplished by defining an adjusted airborne release fraction (AARF) that equals the ARF multiplied by the oxide powder fill fraction:

$$AARF = ARF\left(\frac{V_s}{V_t}\right) \tag{33}$$

The AARF has the advantageous feature of remaining relatively constant over a wide range of fill fractions. Fig. 10 depicts a typical variation of the predicted AARF with fill fraction for the high-pressure range, where the powder entrainment is predicted to be enhanced by a sonic shock, and Fig. 11 shows a typical variation at lower pressures, where it is predicted that the mixing is not enhanced. In both cases, the maximum value of the AARF exceeds the value for a filled vessel by about 10%.

The bounding ARF is correlated in terms of the bounding AARF by

$$ARF_{max} = AARF_{max}\left(\frac{V_t}{V_s}\right) \tag{34}$$

The bounding AARF, in turn, is calculated as the maximum value over the range of powder fill fractions:

$$AARF_{max} = max\left(AARF\right) \tag{35}$$

A sufficiently accurate bound is obtained by evaluating the fill fraction at intervals of 5%, as illustrated in Figs. 9 and 10.

The bounding AARF at pressures above the threshold where a sonic shock is predicted to occur (0.329 MPa or 33.0 psig), is modified to account for variations in entrainments measured by Sutter et al. This modification takes the form

$$AARF_{95\%} = \left(\frac{1}{2} \frac{W_s}{W_g} \bigg|_{95\%} \right) AARF_{max} \tag{36}$$

The factor 1/2 in Eq. 36 represents the inverse of the predicted entrainment ratio at high pressures.

The predicted values for the AARF can be correlated as linear functions of the gauge pressure, as shown by Figs. 12 and 13. The intercepts from these linear regressions are increased slightly to generate an upper bound for all calculated values of the AARF. The resulting correlations for higher pressures, above the threshold where a sonic shock is predicted to enhance entrainment, and for lower pressures, below this threshold, are given by

$$AARF_{HP} = 0.00364 + 0.00379 P_{ga} \tag{37}$$

and

$$AARF_{LP} = 0.000225 + 0.000916 P_{ga} \tag{38}$$

CONCLUSIONS

Results from Pressurized Airborne Release Experiment (PARE) tests conducted at PNL are used to develop correlations to predict airborne release fractions (ARFs) for PuO_2 powder with adsorbed moisture. Results from these tests indicate that entrainment of powder particles into the gas released during a vessel rupture is enhanced due to a sonic shock in the gas. Calculations show that this shock is present if the pressure prior to the rupture exceeds 0.329 MPa (33 psig). The amount of powder that becomes airborne is correlated in terms of an adjusted airborne release fraction (AARF) equal to the product of the ARF and the ratio of the total vessel volume to the volume occupied by the powder bed. For releases of PuO_2 particles with adsorbed moisture, the AARF is correlated as a function of the gauge pressure prior to the vessel rupture. The agreement between the predicted and measured entrainment fractions for the PNL PARE tests leads to the conclusion that these tests were representative of releases following a vessel rupture.

The ARF correlations presented in this study are specific to pressurization of PuO_2 powder due to heating and evaporation of adsorbed moisture. In general, the ARF increases when the gas density inside the vessel increases or the powder particle (pycnometric) density decreases. Therefore, the ARF correlations conservatively overestimate the entrained powder fraction for a vessel bursting due to a hydrogen deflagration, for which the gas temperature would be much higher and the gas density would be much lower.

FUNDING

This manuscript has been authored by Savannah River Nuclear Solutions, LLC under Contract No. DE-AC09-08SR22470 with the U.S. Department of Energy. The United States Government retains and the publisher, by accepting this article for publication, acknowledges that the United States Government retains a non-exclusive, paid-up, irrevocable, worldwide license to publish or reproduce the published form of this work, or allow others to do so, for United States Government purposes.

NOMENCLATURE

A, B, C	Antoine equation parameters
$AARF$	airborne release fraction, adjusted for the presence of a gas space in the vessel
$AARF_{max}$	maximum adjusted airborne release fraction for any powder fill fraction
$AARF_{95\%}$	upper bound adjusted airborne release fraction, at the 95% one-sided confidence level
$AARF_{HP}$	adjusted airborne release fraction at high pressures (above 0.329 MPa (33.0 psig))
$AARF_{LP}$	adjusted airborne release fraction at low pressures (below 0.329 MPa (33.0 psig))
ARF_{max}	maximum airborne release fraction for any powder fill fraction
ARF	airborne release fraction for powder
c	sonic velocity of gas
c_p	constant pressure gas specific heat
h	enthalpy of flowing gas
h_0	stagnation enthalpy of the gas
k	ratio of constant pressure to constant volume specific heat
M	Mach number
M_{air}	molecular mass of air
m_f	effectiveness factor for mixing of powder with gas in the volume free space
m_g	mass of gas in the vessel
M_{H_2O}	molecular mass of water
$max(AARF)$	maximum adjusted airborne release fraction over the range of powder fill fractions, determined from tabulations at fill fraction increments of 0.05
P	downstream pressure of the flowing gas
P_0	stagnation pressure
P_a	ambient pressure (packaging pressure)
P_{air}	partial pressure of air
P_{ga}	gauge pressure, MPA or psig
P_{v,H_2O}	water vapor pressure, MPa or psia
P_{v,H_2O}	partial pressure of water vapor
R_g	ideal gas constant
s_f	slip ratio
T	downstream temperature of the flowing gas

T_0 stagnation temperature

T_a ambient temperature (packaging temperature)

T_r reference temperature, 273.15 K

v_g gas velocity

V_s bulk volume of powder in the vessel

v_s velocity of solids

V_t total vessel volume

W_s mass flow rate of solids

W_g mass flow rate of gas

$\left.\dfrac{W_s}{W_g}\right|_{95\%}$ bounding ratio of entrained powder to gas mass flow rate, at the 95% one-sided confidence level

$\left.\dfrac{W_s}{W_g}\right|_{95\%,P_i}$ bounding ratio of entrained powder to gas mass flow rate, at the 95% one-sided confidence level, at a single pressure P_i

$\left\langle\dfrac{W_s}{W_g}\right\rangle_{P_i}$ average ratio of entrained powder to gas mass flow rate, at a single pressure P_i

ε powder void fraction

$\rho_{g,0}$ stagnation density of the gas

ρ_s pycnometric density of solid powder

$\sigma\left(\dfrac{W_s}{W_g}\right)_{P_i}$ standard deviation of entrained powder to gas mass flow rate, at a single pressure P_i

REFERENCES

[1] DOE-HDBK-3010-94, 1994, "DOE Handbook: Airborne Release Fractions/Rates and Respirable Fractions for Nonreactor Nuclear Facilities."

[2] Sutter, S. L., 1983, "Aerosols Generated by Releases of Pressurized Powders and Solutions in Static Air," U. S. Nuclear Regulatory Commission Report NUREG/CR-3093, Pacific Northwest Laboratory Report PNL-4566.

[3] Sutter, S. L., 1983, "Powder Aerosols Generated by Accidents: Pressurized Release Experiments," Am. Ind. Hyg. Assoc. J., 44(6), pp. 379-383.

[4] Ballinger, M. Y., Sutter, S. L., and Hodgson, W. H., 1987, "New Data for Aerosols Generated by Releases of Pressurized Powders and Solutions in Static Air," U. S. Nuclear Regulatory Commission Report NUREG/CR-4779, Pacific Northwest Laboratory Report PNL-6065.

[5] Matsen, J. M., 1982, "Mechanisms of Choking and Entrainment," Powder Technol., 32(1), pp. 21-33.

[6] Van Wylen, G. J. and Sonntag, R. E., 1973, <u>Fundamentals of Classical Thermodynamics,</u> <u>2nd ed.,</u> John Wiley and Sons, Inc., New York, Chapter 14.

[7] <u>CRC Handbook of Chemistry and Physics, 75th ed.,</u> 1994, CRC Press, Boca Raton, Florida, p. A-105.

[8] Speight, J. G., 2018, <u>Formulas and Calculations for Drilling Operations</u>, John Wiley & Sons, Inc., Hoboken, New Jersey, Section 1.05.

Table 1. Results of PARE tests with high powder loading in chamber (0.350 kg)

Gauge Pressure, MPa (psi)	Mass Entrained Powder, kg	
	TiO$_2$	**U$_3$O$_8$**
3.45 (500)	0.0278	0.0302
1.72 (250)	0.0183	0.0205
0.345 (50)	0.0033	0.0069
0.169 (24.5)	----	0.00061
0.121 (17.5)	----	0.00039
0.062 (9)	----	0.00002

Table 2. Results of PARE tests with low powder loading in chamber (0.100 kg)

Gauge Pressure, MPa (psi)	Mass Entrained Powder, kg	
	TiO$_2$	**U$_3$O$_8$**
3.45 (500)	0.0241	0.0198
1.72 (250)	0.0182	0.0130
0.345 (50)	0.0044	0.0036
0.169 (24.5)	----	0.00030
0.121 (17.5)	----	0.00006
0.062 (9)	----	0.00003
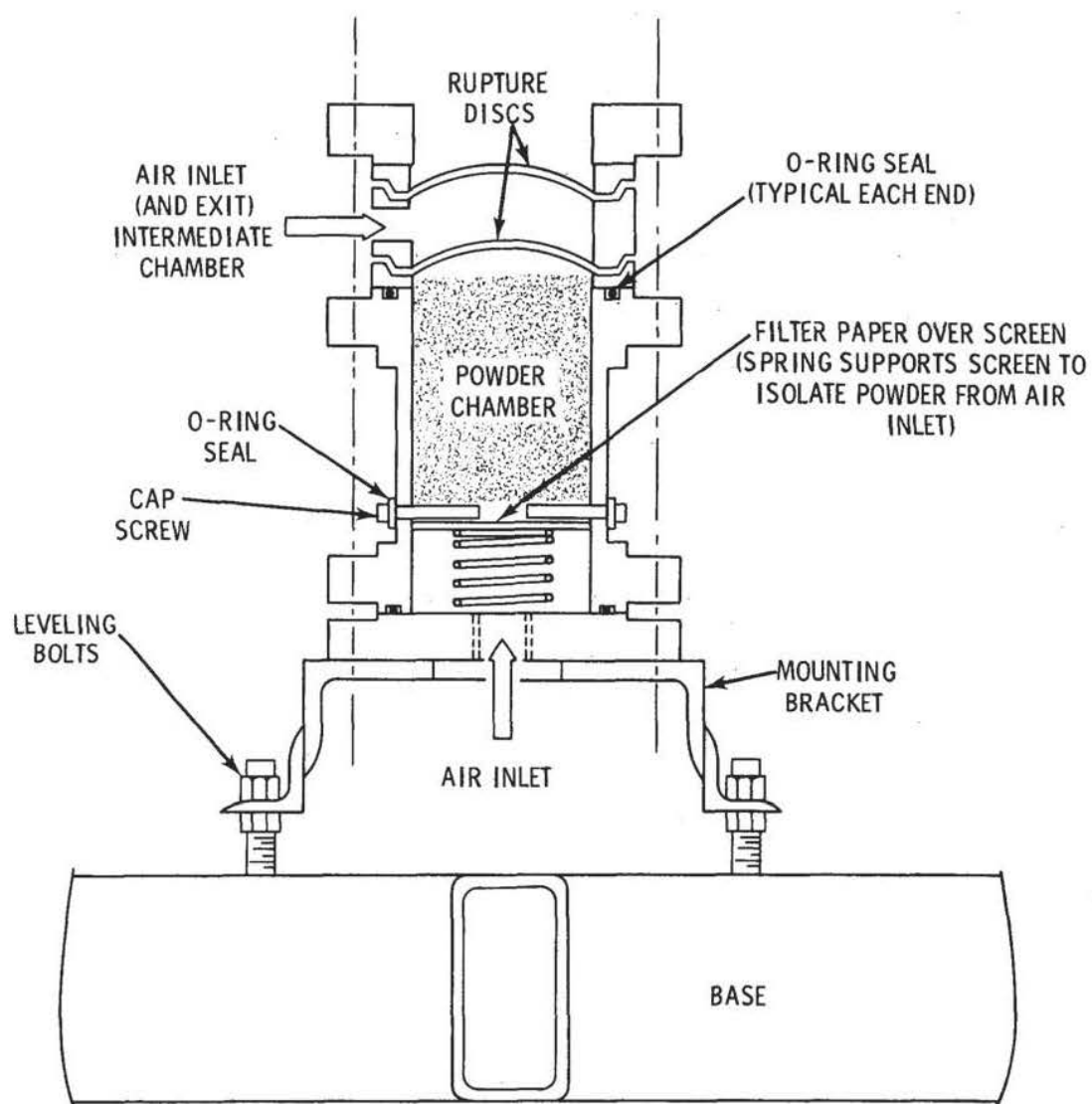
Fig. 1. Schematic of PARE apparatus (from Ref. [2])
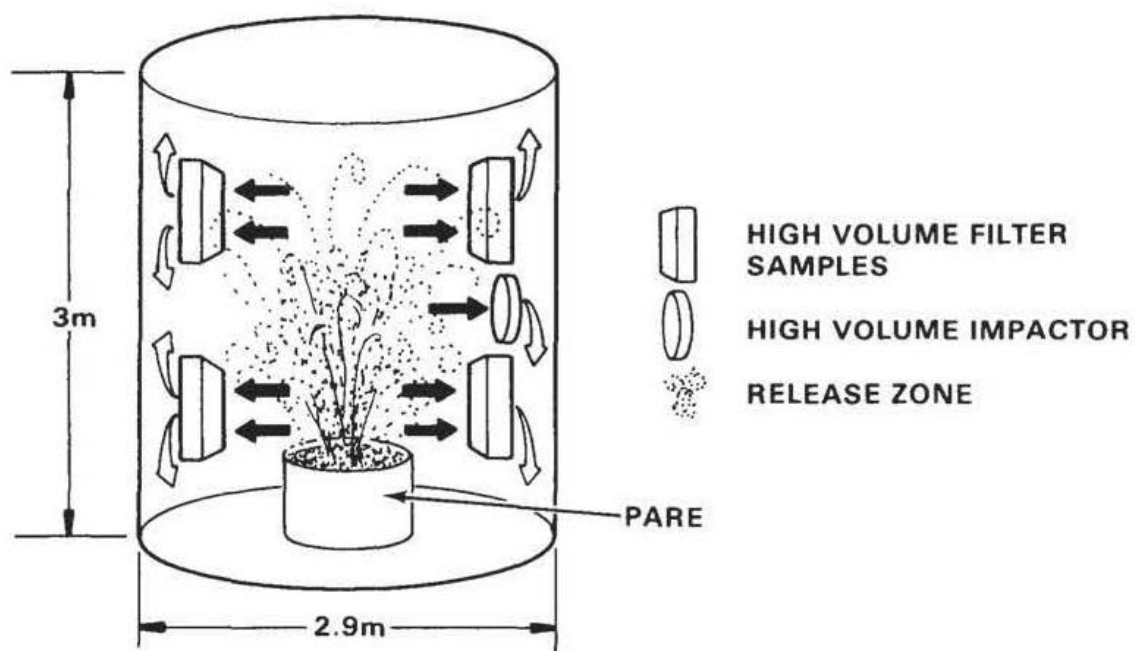
Fig. 2. PARE sample collection (from Ref. [2])
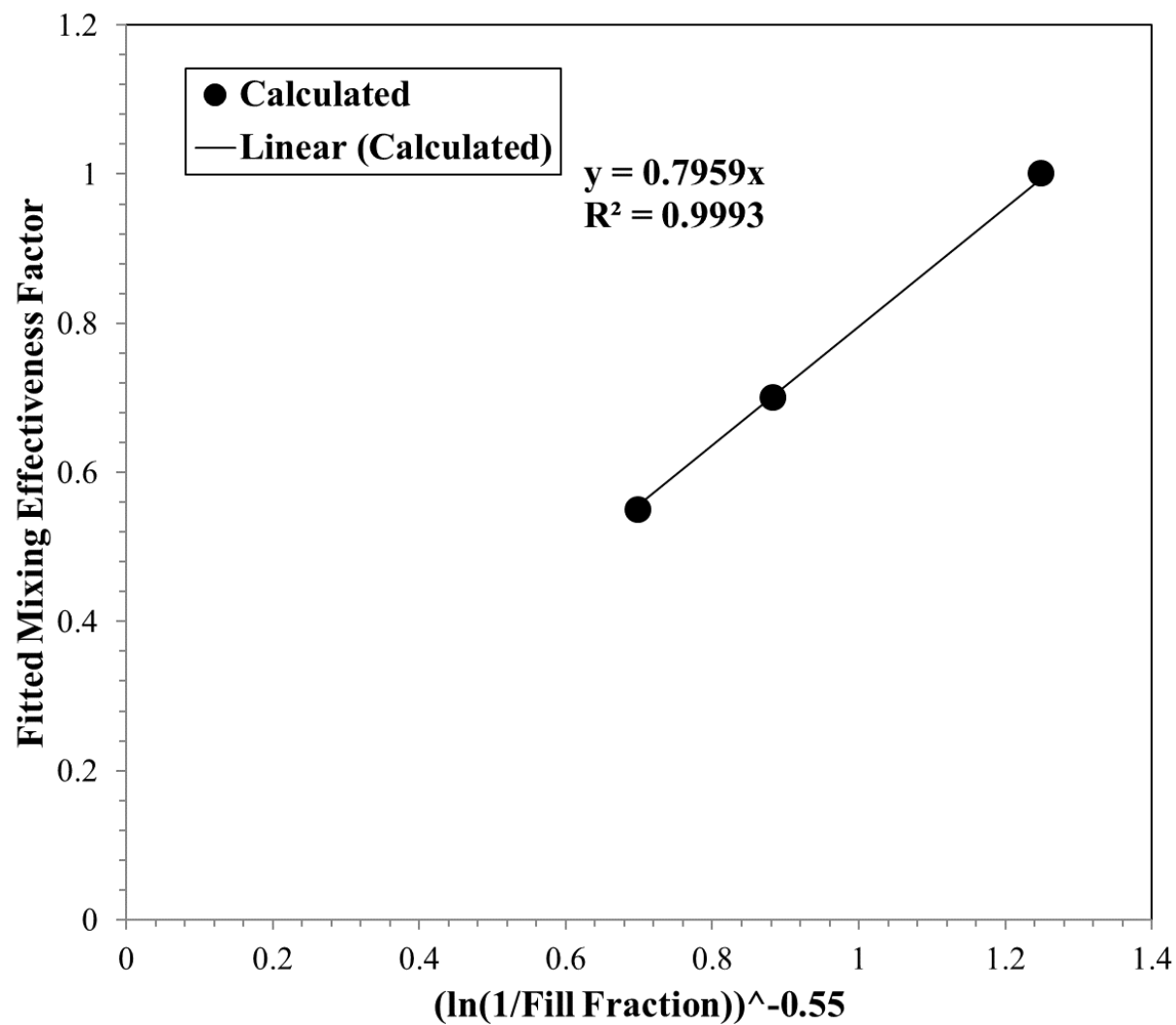
Fig. 3. Mixing effectiveness factors for PNL PARE tests
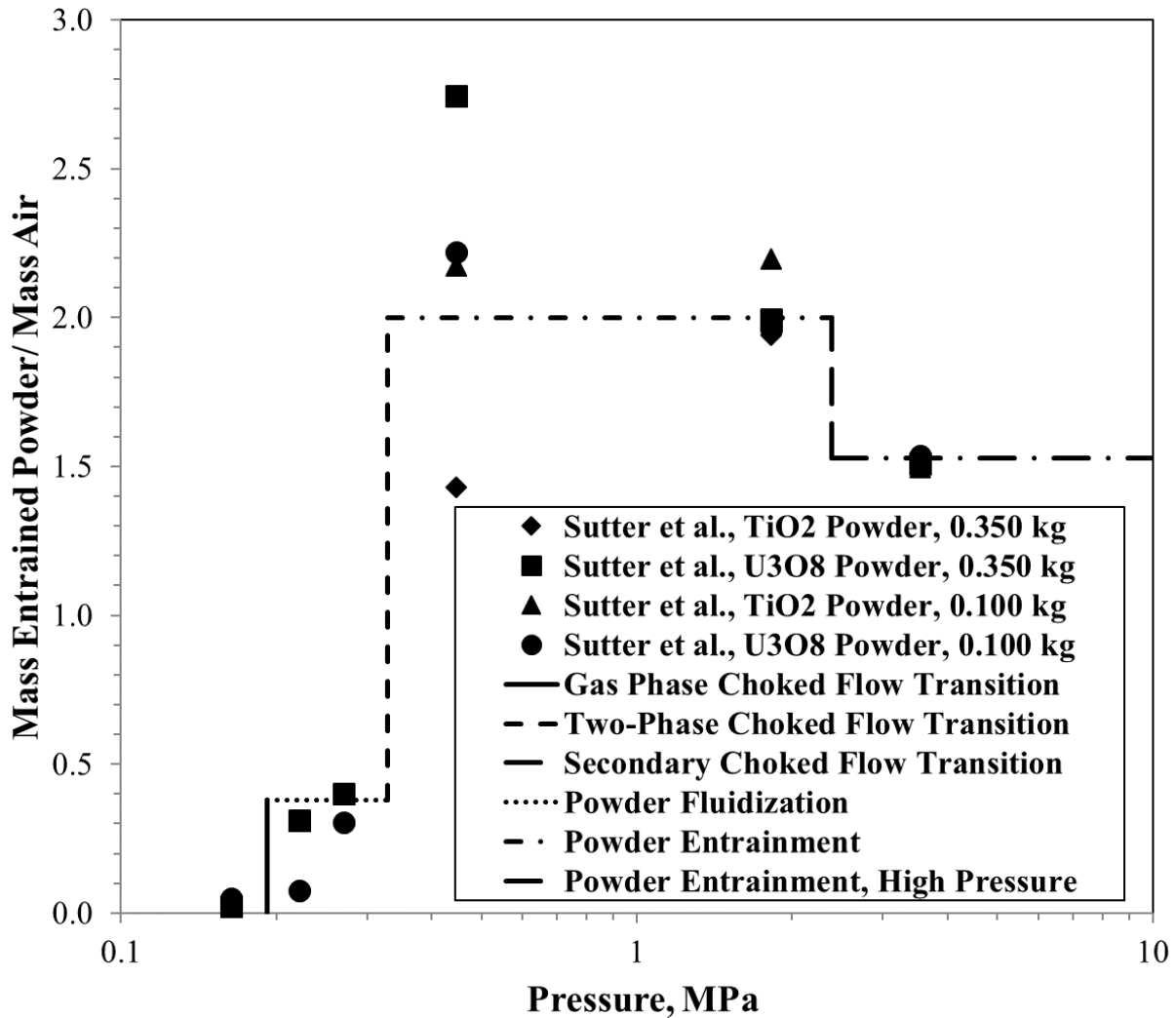
Fig. 4. Comparison of measured and predicted entrainments for PNL PARE tests

$$y = 0.5059x^{-0.964}$$
$$R^2 = 1$$
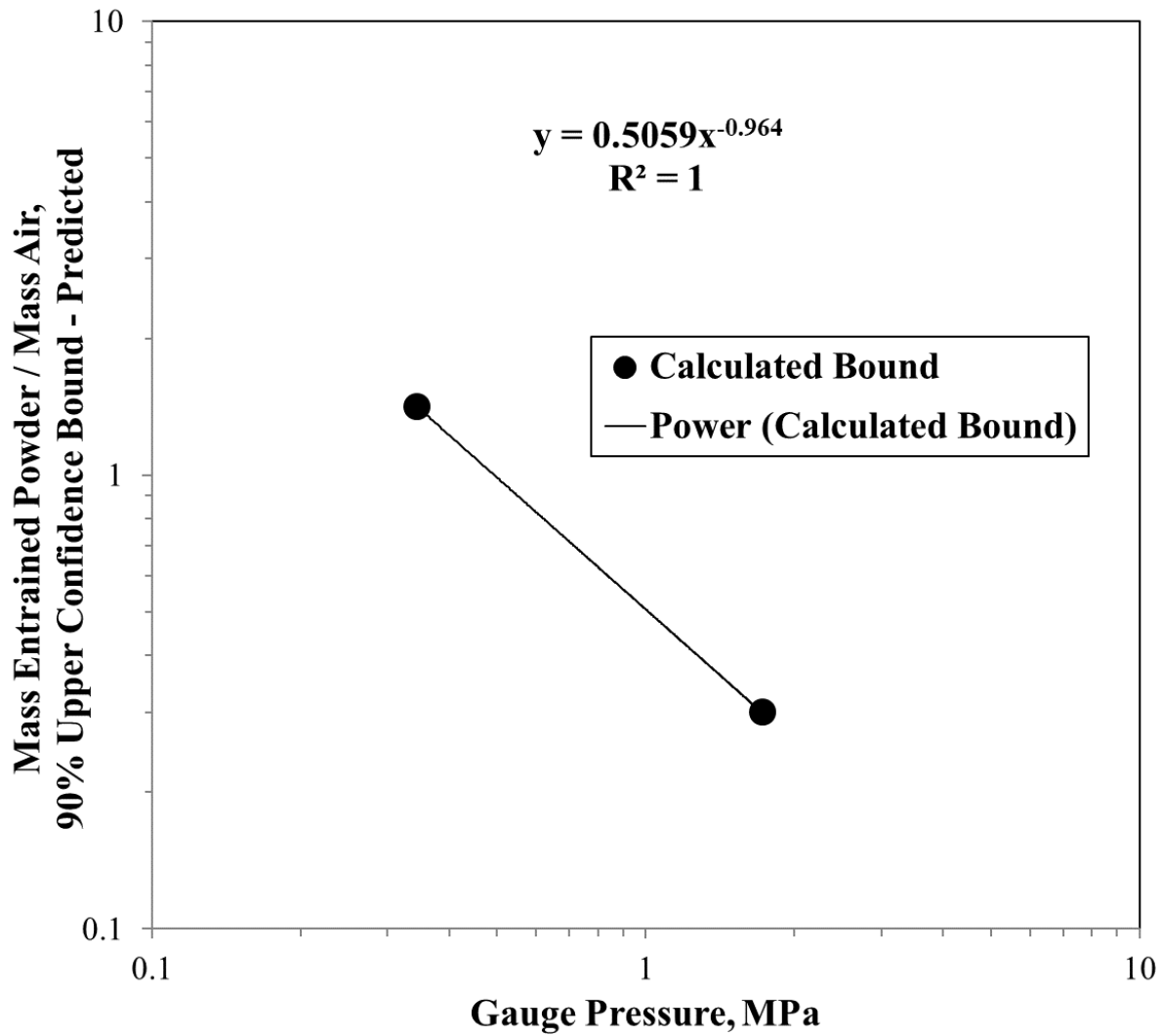
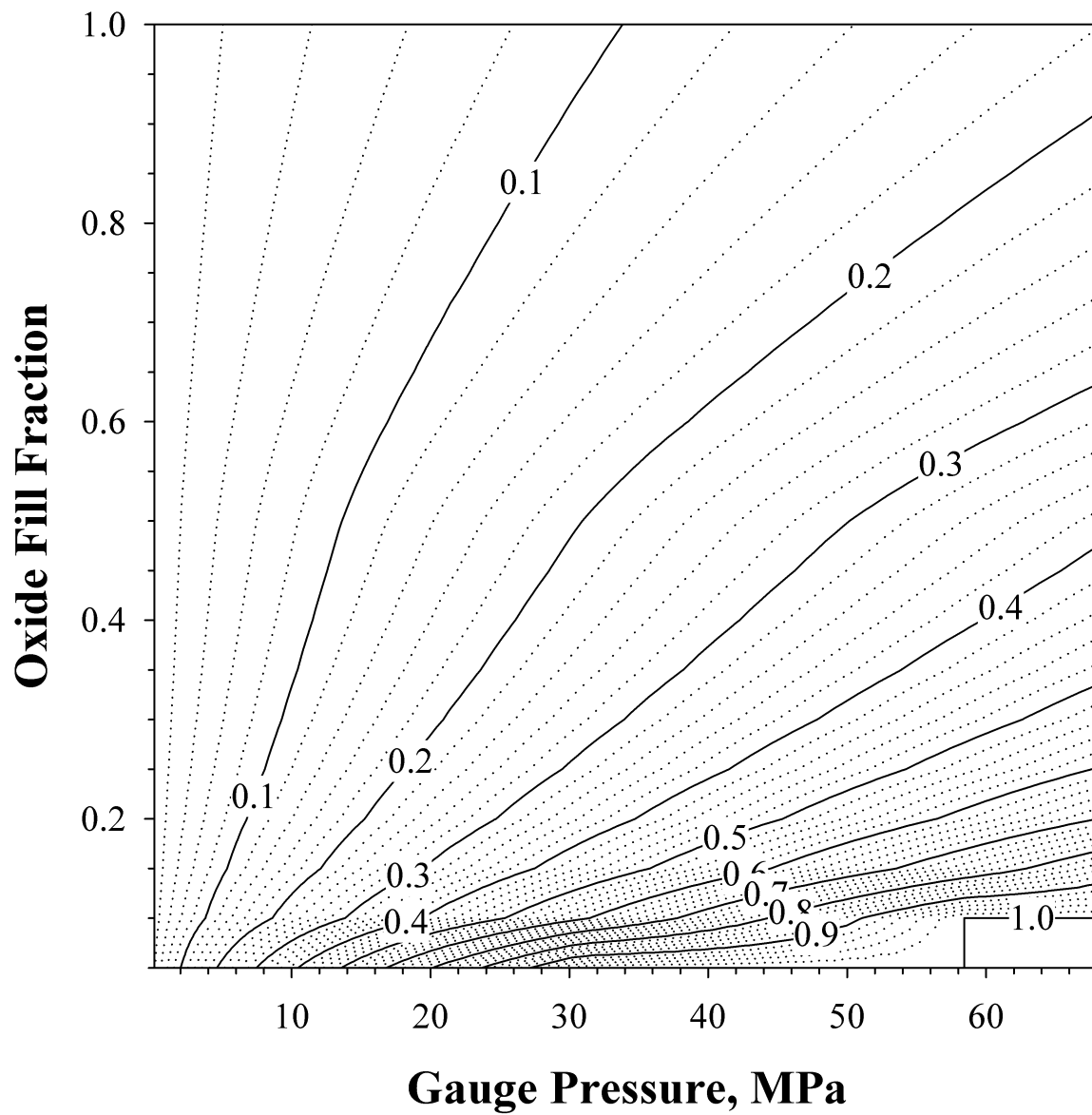Fig. 5. Correlation of upper confidence bound for powder entrainment ratio
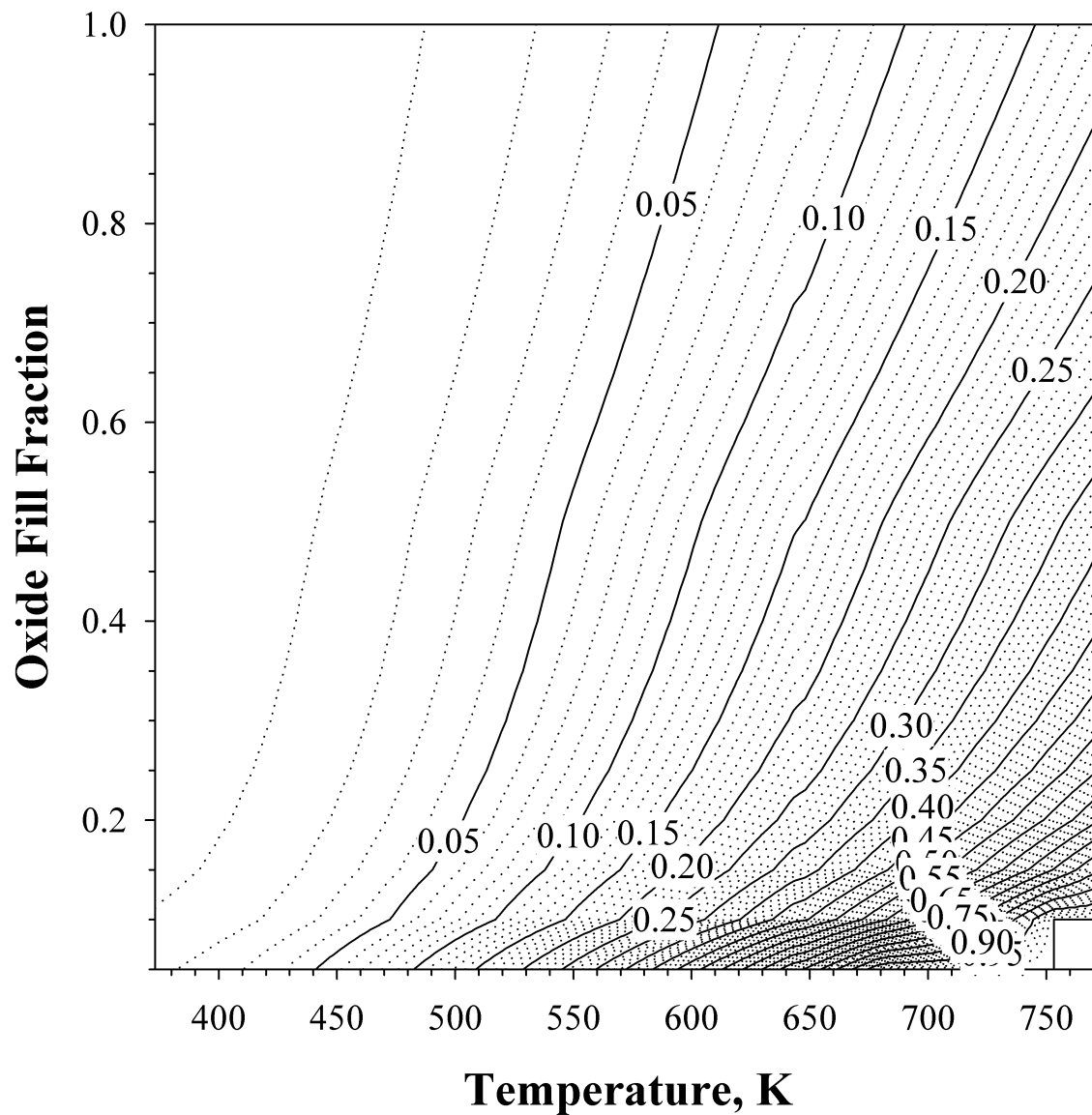
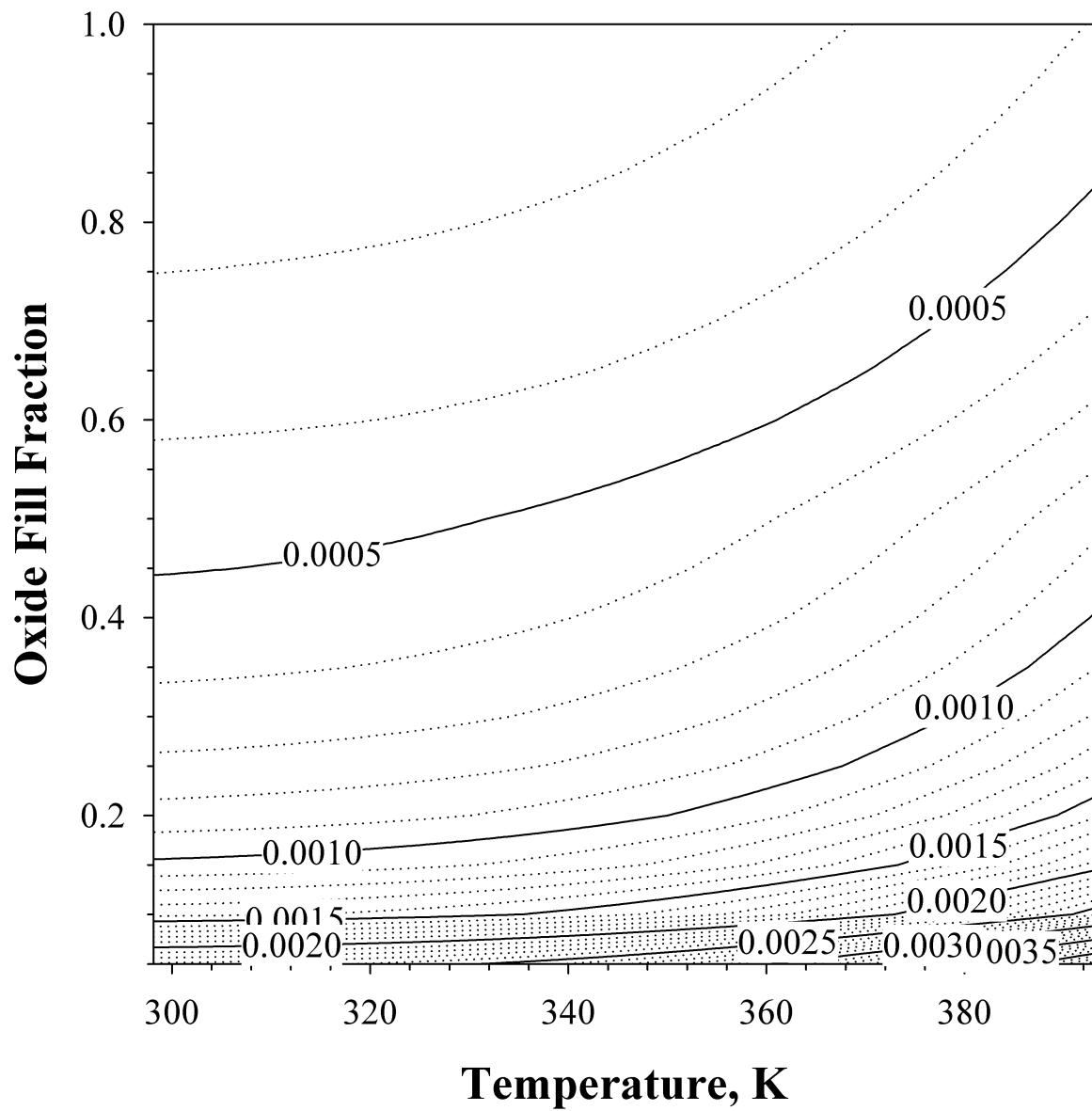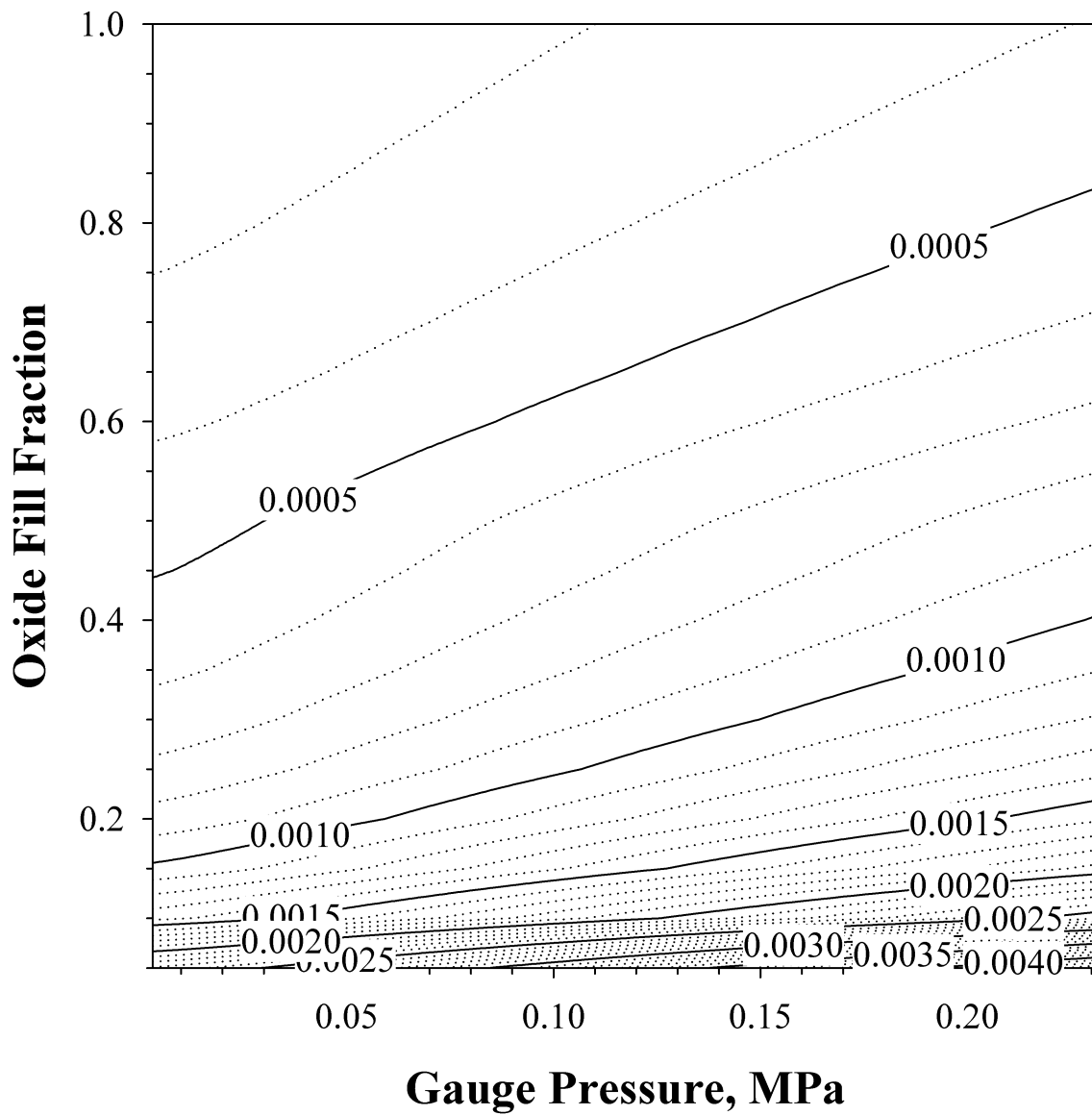**Fig. 6. Airborne release fractions for venting of a vial containing saturated air and plutonium oxide powder, high temperature range**

Fig. 7. Airborne release fractions for venting of a vial containing saturated air and plutonium oxide powder, low temperature range

Fig. 8. **Airborne release fractions for venting of a vial containing saturated air and plutonium oxide powder, high pressure range**

Fig. 9. Airborne release fractions for venting of a vial containing saturated air and plutonium oxide powder, low pressure range
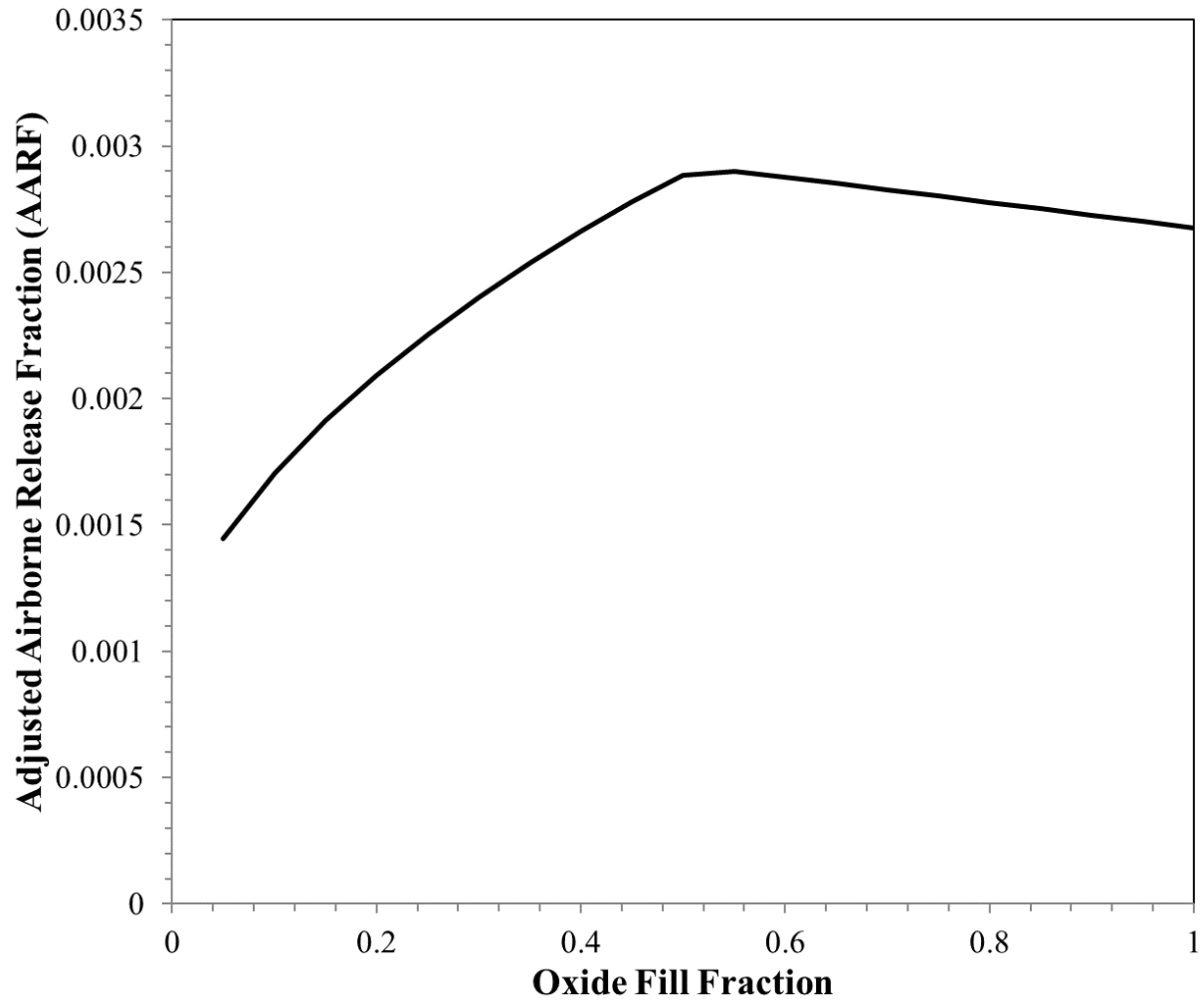
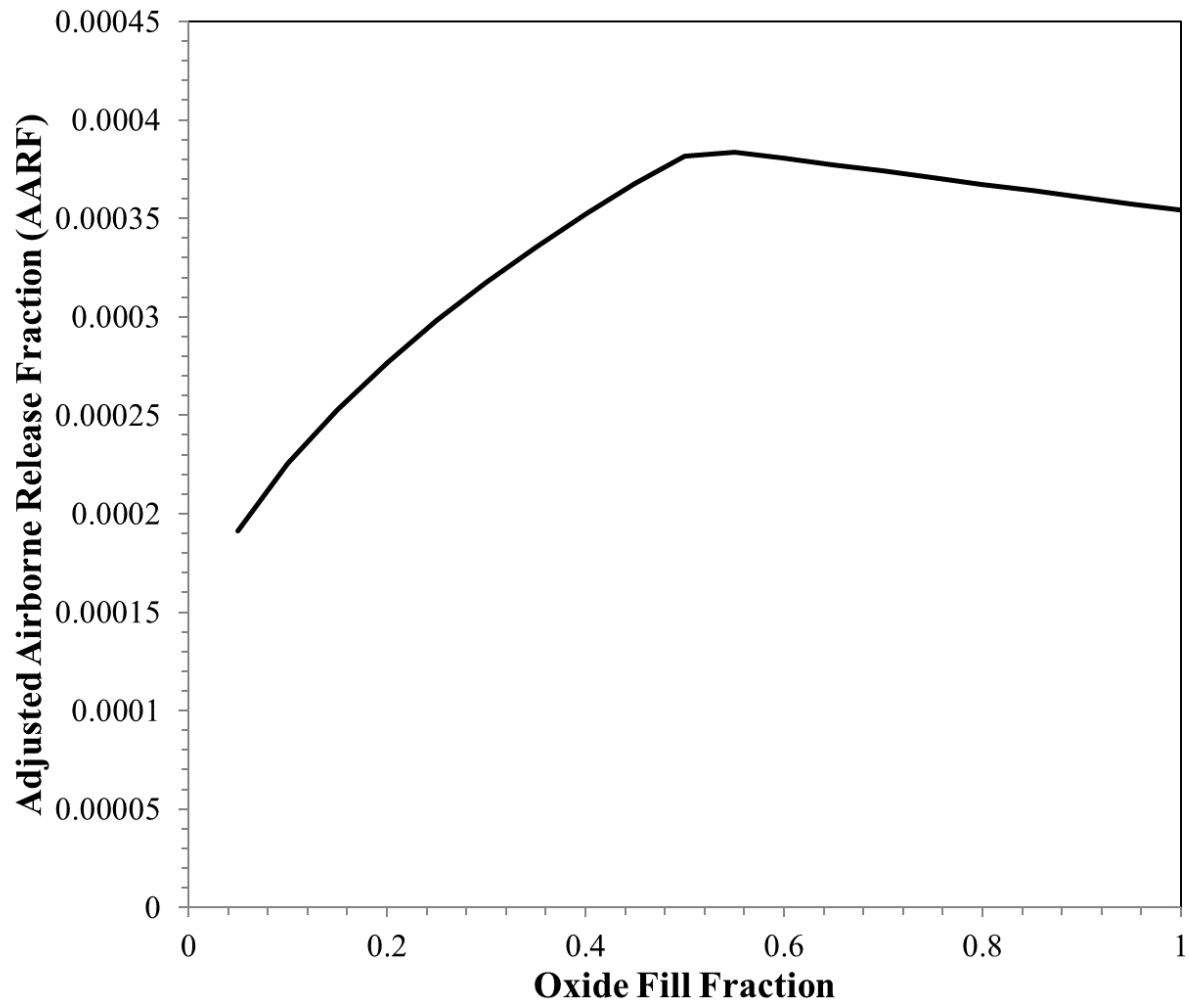Fig. 10. Variation of ARF with oxide fill fraction at 0.454 MPa (51.2 psig) (408 K)

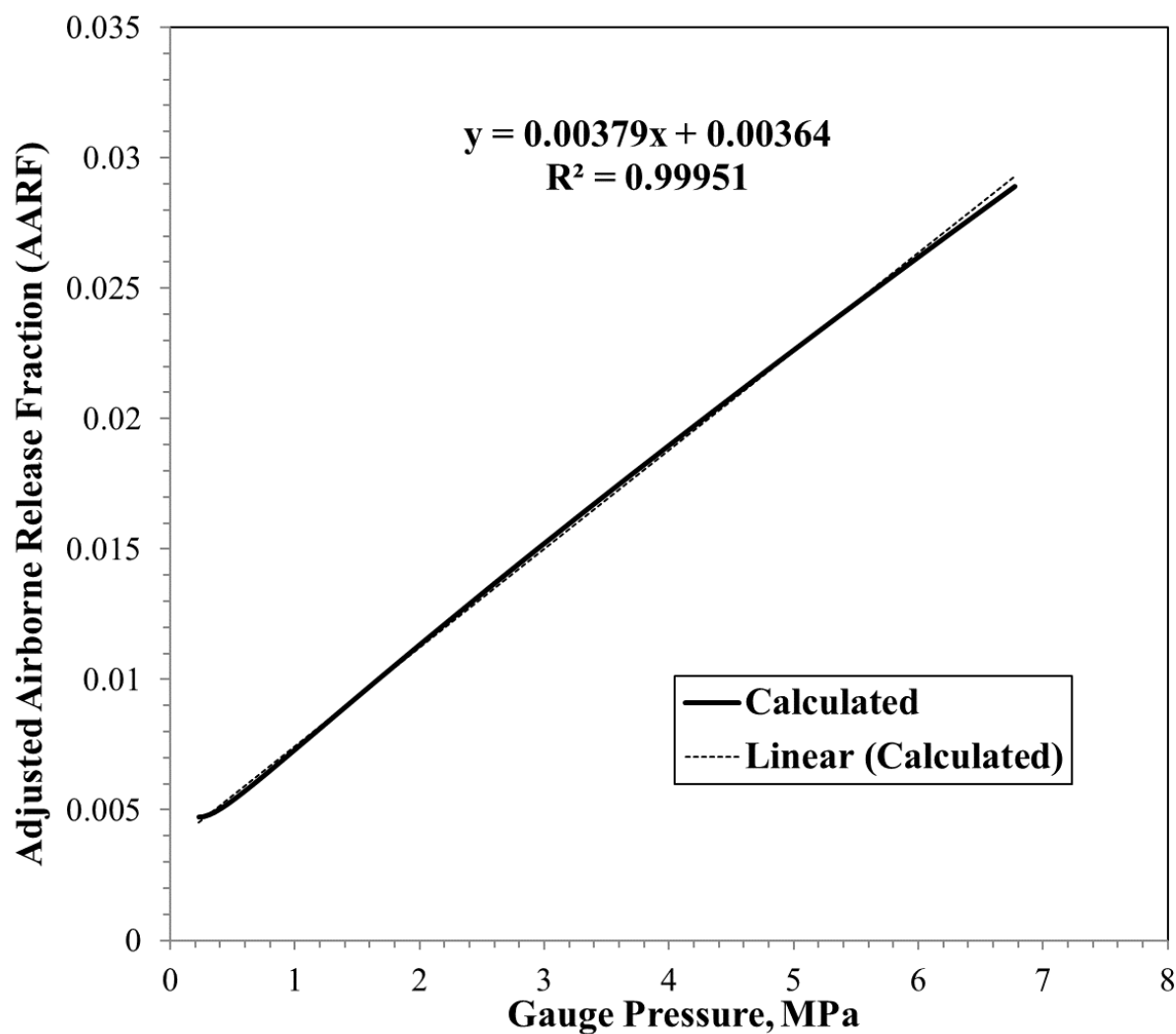**Fig. 11. Variation of ARF with oxide fill fraction at 0.274 MPa (25 psig) (383 K)**

Fig. 12. Correlation of adjusted ARF at high pressures (> 0.329 MPa (33.0 psig))
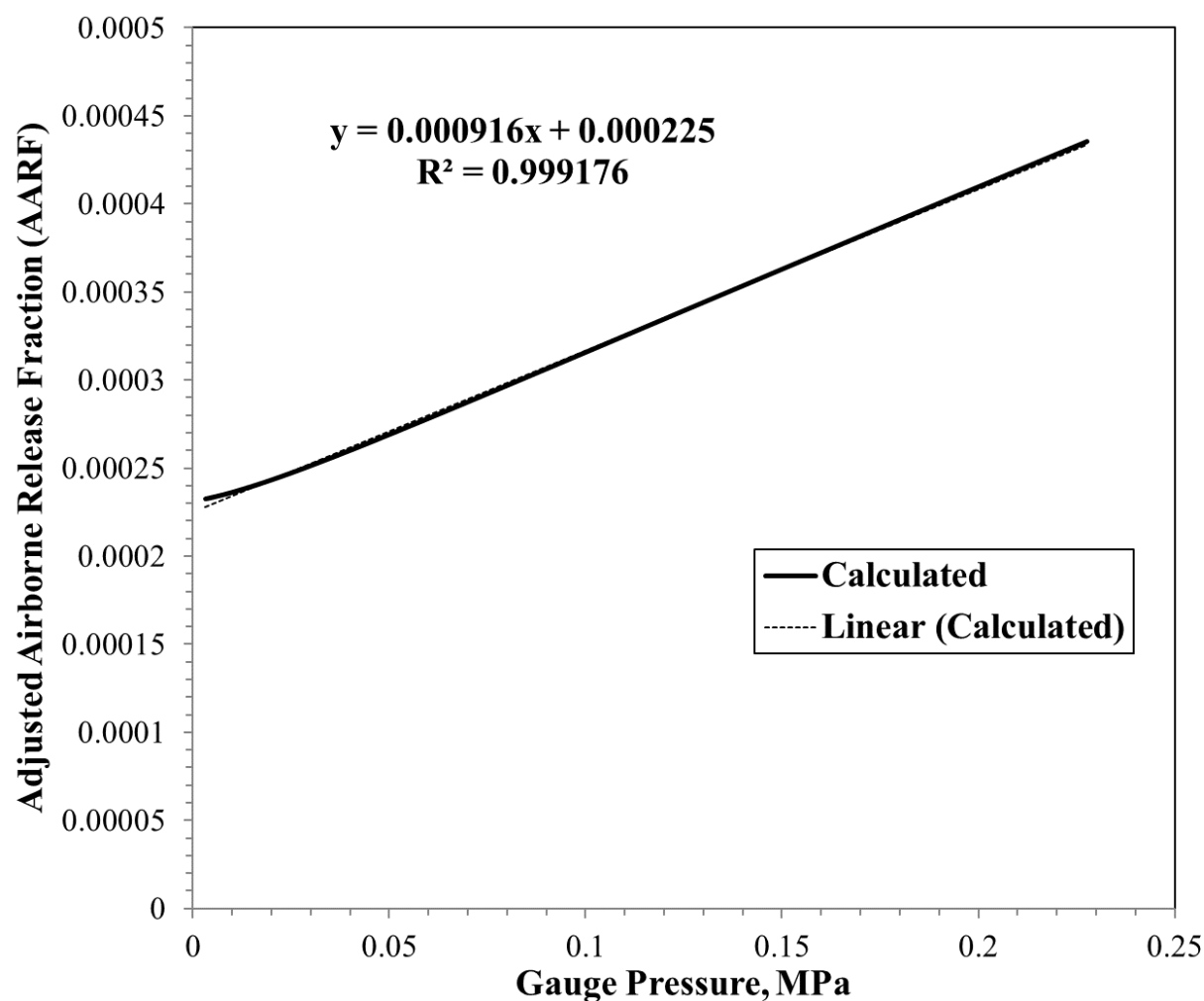
Fig. 13. Correlation of adjusted ARF at low pressures (< 0.329 MPa (33.0 psig))